



1 **Full-coverage 1 km daily ambient PM_{2.5} and O₃ concentrations of China in**
2 **2005-2017 based on multi-variable random forest model**

3

4 Runmei Ma^{1#}, Jie Ban^{1#}, Qing Wang^{1#}, Yayi Zhang¹, Yang Yang², Shenshen Li³,
5 Wenjiao Shi^{4,5}, Tiantian Li^{1*}

6

7 ¹ China CDC Key Laboratory of Environment and Population Health, National Institute of
8 Environmental Health, Chinese Center for Disease Control and Prevention, Beijing, 100021,
9 China

10 ² Institute of Urban Meteorology, China Meteorological Administration, Beijing, 100089,
11 China

12 ³ State Key Laboratory of Remote Sensing Science, Institute of Remote Sensing and Digital
13 Earth, Chinese Academy of Sciences, Beijing, 100101, China

14 ⁴ Key Laboratory of Land Surface Pattern and Simulation, Institute of Geographic Sciences
15 and Natural Resources Research, Chinese Academy of Sciences, Beijing 100101, China

16 ⁵ College of Resources and Environment, University of Chinese Academy of Sciences,
17 Beijing 100049, China

18

19 # Runmei Ma, Jie Ban and Qing Wang are the co-first authors.

20 * Corresponding author: E-mail: litiantian@nieh.chinacdc.cn



21 **Abstract**

22 The health risks of fine particulate matter (PM_{2.5}) and ambient ozone (O₃) have been
23 widely recognized in recent years. An accurate estimate of PM_{2.5} and O₃ exposures is
24 important for supporting health risk analysis and environmental policy-making. The
25 aim of our study was to construct random forest models with high-performance, and
26 estimate daily average PM_{2.5} concentration and O₃ daily maximum 8h average
27 concentration (O₃-8hmax) of China in 2005-2017 at a spatial resolution of 1km×1km.
28 The model variables included meteorological variables, satellite data, chemical
29 transport model output, geographic variables and socioeconomic variables. Random
30 forest model based on ten-fold cross validation was established, and spatial and
31 temporal validations were performed to evaluate the model performance. According
32 to our sample-based division method, the daily, monthly and yearly simulations of
33 PM_{2.5} gave average model fitting R² values of 0.85, 0.88 and 0.90, respectively; these
34 R² values were 0.77, 0.77, and 0.69 for O₃-8hmax, respectively. The meteorological
35 variables and their lagged values can significantly affect both PM_{2.5} and O₃-8hmax
36 simulations. During 2005-2017, PM_{2.5} exhibited an overall downward trend, while
37 ambient O₃ experienced an upward trend. Whilst the spatial patterns of PM_{2.5} and
38 O₃-8hmax barely changed between 2005 and 2017, the temporal trend had spatial
39 characteristic. The dataset is accessible to the public at
40 <https://doi.org/10.5281/zenodo.4009308> (Ma et al., 2021), and the shared data set of
41 Chinese Environmental Public Health Tracking: CEPHT
42 (<https://cepht.niehs.cn:8282/developSDS3.html>).



43 **1 Introduction**

44 Air pollution is becoming a main concern of modern society due to various health
45 risks. According to the latest Global Burden of Disease (GBD) report, air pollution
46 has caused approximately 6.67 million deaths (95% UI: 5.90-7.49 million), and
47 ranked fourth on the global list of death-related risk factors in 2019 (Health Effects
48 Institute, 2020; Murray et al., 2020). Ambient fine particulate matter (PM_{2.5}) and
49 ambient ozone (O₃) have been identified and proven to be related to many health
50 outcomes. China is known to be one of the countries with the most serious air
51 pollution in the world. Strict pollution control measures (including *the Air Pollution*
52 *Prevention and Control Action Plan* and *three-year action plan to fight air pollution*)
53 were enacted by the Chinese government in order to control and reduce serious air
54 pollution since 2013. The implementation of these measures has resulted in a
55 markable drop of emissions and PM_{2.5} concentration. Nonetheless, the occasional
56 haze and unsatisfactory O₃ pollution control effects in 2013-2017, as well as the short
57 development history of air quality monitoring network, have brought many
58 difficulties to accurately capture the temporal and spatial patterns of PM_{2.5} and O₃
59 concentrations. Therefore, it is difficult to develop a complete decision-making basis
60 for handling air pollution. In addition, there are gaps in epidemiological studies
61 linking air pollutants to health outcomes, due to the lack of accurate measurements of
62 PM_{2.5} and ambient O₃ concentrations. To this end, an accurate estimate of PM_{2.5} and
63 O₃ exposures is essential to support health risk analysis and environmental
64 policy-making.



65

66 Suitable model variables and advanced simulation method are important to achieve
67 accurate modeling. Basically, $PM_{2.5}$ is jointly affected by both natural conditions and
68 human activities over space and time, e.g., Aerosol Optical Depth (AOD),
69 meteorological conditions, geographic factors and human-related features (Wei et al.,
70 2021). While O_3 is a secondary pollutant, which is produced by a series of complex
71 photochemical reactions on the basis of precursor including nitrogen oxides (NO_x)
72 and volatile organic compounds (VOCs) under the action of high temperature and
73 strong radiation. These complex characteristic puts forward higher requirements on
74 the ability of the modeling method to handle multi-variable, and capture the
75 non-linear relationships between variables and air pollutants. Many models have been
76 developed to simulate the spatiotemporal distribution of $PM_{2.5}$ and O_3 concentrations
77 in China. Machine-learning approaches (e.g., random forest (RF), extreme gradient
78 boosting and deep belief network models) can mine useful information from a large
79 amount of input data and explore the nonlinear relationship, leading to a better
80 performance in modeling work(Chen et al., 2018, 2019; Di et al., 2017; Li et al., 2017;
81 Wei et al., 2019; Zhan et al., 2018). However, most of these simulation datasets
82 cannot balance long time series and high spatiotemporal resolution. Besides, there is
83 no long-term simulation dataset for both $PM_{2.5}$ and O_3 concentrations with high
84 temporal and spatial resolution for supporting epidemiological research. Therefore, by
85 incorporating multi-source data into random forest models, this study makes an
86 attempt to simulate the high-resolution ($1km \times 1km$) ambient $PM_{2.5}$ and O_3

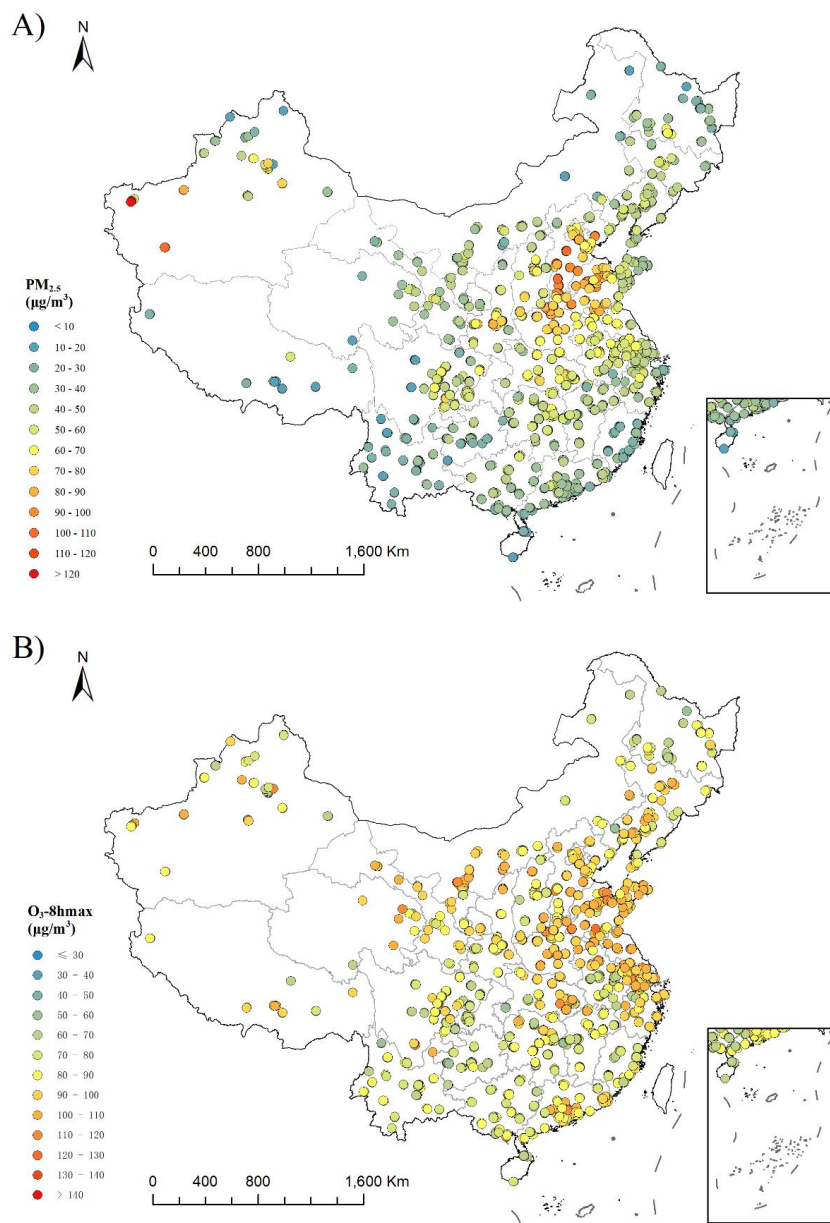


87 concentrations of China in 2005-2017.

88

89 **2. Method**

90 The model variables of this study include meteorological variables, geographical
91 variables, socio-economic variables, satellite data and chemical transport model
92 output in 2013-2017. Daily average $PM_{2.5}$ and O_3 daily maximum 8h average
93 concentration (O_3 -8hmax) monitoring data of 1479 sites in 2013-2017 was obtained
94 (Fig. 1). A $1km \times 1km$ standard grid is created across the country (35.55° N to 43.12°
95 N, and 112.95° E to 120.35° E) with a total of 9495025 grid cells. The coordinate
96 system of the grid is WGS-84. We construct high-performance random forest (RF)
97 models (temporal resolution: daily; spatial resolution: $1km \times 1km$), and simulate the
98 grid daily average $PM_{2.5}$ concentration and O_3 -8hmax concentration of China in
99 2005-2017.



100
101 **Fig.1 Station distribution in China and average ground monitoring concentration of $PM_{2.5}$**
102 **(A) and $O_3-8hmax$ (B) from 2013 to 2017**

103

104 **2.1 Data set**



105 The model variables used in this study mainly include Aqua AOD (Aerosol Optical
106 Depth) for PM_{2.5} modeling, GEOS-Chem chemical transport model output for O₃
107 modeling, and some variables shared by PM_{2.5} and O₃: 13 meteorological variables
108 (includes boundary layer height, surface pressure, 2 meter dew point temperature,
109 evaporation, albedo, low cloud cover, medium cloud cover, high cloud cover, total
110 precipitation, 10 meter U wind component, 10 meter V wind component, 2 meter
111 surface temperature and surface solar radiation downwards) and its lag 1 and lag 2,
112 geographic and socio-economic variables, such as DEM (Digital Elevation Model),
113 NDVI (Normalized Difference Vegetation Index), population, GDP (Gross Domestic
114 Product), road network and dummy variables (includes season, month, and spatial
115 dummy variables, province). A more detailed description of the model variables is
116 given in Table S1. The processing method has been described in detail in our earlier
117 studies (Ma et al., 2021; Zhao et al., 2019). Briefly, most of the model variables are
118 processed into 1km×1km resolution based on the standard grid using interpolation
119 methods (such as inverse distance weighted and bilinear algorithm) in ArcGIS 10.2
120 and Python 2.7. For the long-term variables, the corresponding monthly and annual
121 level value is assigned to each day. Subsequent modeling work was carried out based
122 on the data set that covering monitoring data and all variables.

123

124 **2.2 Random forest model**

125 Random forest is an ensemble machine learning method consisting of many
126 individual decision trees growing from bagged data and its prediction is a vote result



127 of those trees (Breiman, 2001). The RF algorithm primarily integrates learning
128 principles, trains several individual learners, and finally forms a strong learner
129 through a certain combination strategy; through multiple rounds of training, multiple
130 prediction results are obtained, and the final results are obtained after average
131 aggregation.

132

133 The random forest models are established using the 10-fold cross validation method.

134 First of all, this method randomly divides the modeling data set into 10 parts; then 9

135 of them are used for modeling, the remaining one is used for simulation and be

136 compared with observations. The verification is repeated until every part is predicted.

137 In this way, the modeling and verification of simulation are repeated 10 times in total,

138 and the average values of the 10 runs is took as the final result, i.e., the CV-R². The

139 formulae of the models are as follows:

140

$$141 \quad PM_{2.5ij} = f(METE_{ij}, lag1METE_{ij}, lag2METE_{ij}, AOD_{ij}, LD_j, ROAD_j, NDVI_j, ELE_j, GDP_j,$$

$$142 \quad POP_j, SEASON_i, MON_i, PRO_j) \quad (1)$$

$$143 \quad O_3-8hmax_{ij} = f(METE_{ij}, lag1METE_{ij}, lag2METE_{ij}, GEOS_{ij}, LD_j, ROAD_j, NDVI_j, ELE_j,$$

$$144 \quad GDP_j, \quad POP_j, \quad SEASON_i, \quad MON_i, \quad PRO_j)$$

$$145 \quad (2)$$

146

147 where $PM_{2.5ij}$ and $O_3-8hmax_{ij}$ are the $PM_{2.5}$ and $O_3-8hmax$ concentrations on day i in

148 grid cell j ; $METE_{i,j}$ is 13 meteorological variables on day i in grid cell j , and lag 1



149 $METE_{ij}$ and $lag2\ METE_{ij}$ represent corresponding one-day lag and two-day lag
150 values, respectively; $GEOS_{ij}$ and $AOD_{i,j}$ are the GEOS-Chem model output and
151 AOD value on day i in grid cell j ; LD_j , $ROAD_j$, $NDVI_j$, ELE_j , GDP_j and POP_j are
152 the land use coverage, length of a variety of roads, NDVI, elevation, GDP and
153 population in grid cell j , respectively; $SEASON_i$, MON_i and PRO_j are the season
154 and month of day i , and province of grid cell j , respectively.

155

156 In general, the random forest parameters that need to be adjusted include $n_estimators$
157 (number of decision trees) and the max_depth (maximum depth of the trees). Unlike
158 the previous methods of manually adjusting parameters, the parameters of random
159 forest were optimized using GridSearchCV, which can realize cross-validated
160 grid-search over a parameter grid. After GridSearchCV, we set max_depth as 36 and
161 $n_estimators$ as 200 for $PM_{2.5}$ modeling. For O_3 -8hmax modeling, we set max_depth
162 as 54 and $n_estimators$ as 200.

163

164 **2.3 Validation method**

165 To comprehensively verify the model performance, we construct the main models
166 using sample-based division method. Models using spatial-based and temporal-based
167 division method are further construct to test the model performance in spatial and
168 temporal scale.

169

170 The data set was randomly divided into training set (90% of the records) and test set



171 (10% of the records) by using the sample-based division method. We construct the
172 main model using the training set with a 10-fold cross-validation. Since the data in the
173 test set is not used in the main model, "true model performance" can be verified. The
174 coefficient of determination (R^2) of main model on test set (test- R^2), and the
175 verification indicators of model uncertainty, the root mean square error (RMSE) and
176 mean absolute error (MAE) are calculated for the $PM_{2.5}$ and O_3 -8hmax model,
177 respectively. The monthly and yearly R^2 are also calculated.

178

179 For the spatial verification, 90% of the monitoring stations are randomly selected. The
180 monitoring data of these stations is used as the training set, and the monitoring data of
181 remaining stations is used as the testing set. For the temporal verification, all date in
182 2013-2017 is randomly divided into nine and one, and the data in these dates is used
183 as training and test sets, respectively. After that, the test- R^2 , RMSE and MAE are
184 calculated.

185

186 **2.4 Simulation of daily $PM_{2.5}$ and ambient O_3 of China from 2005 to 2017**

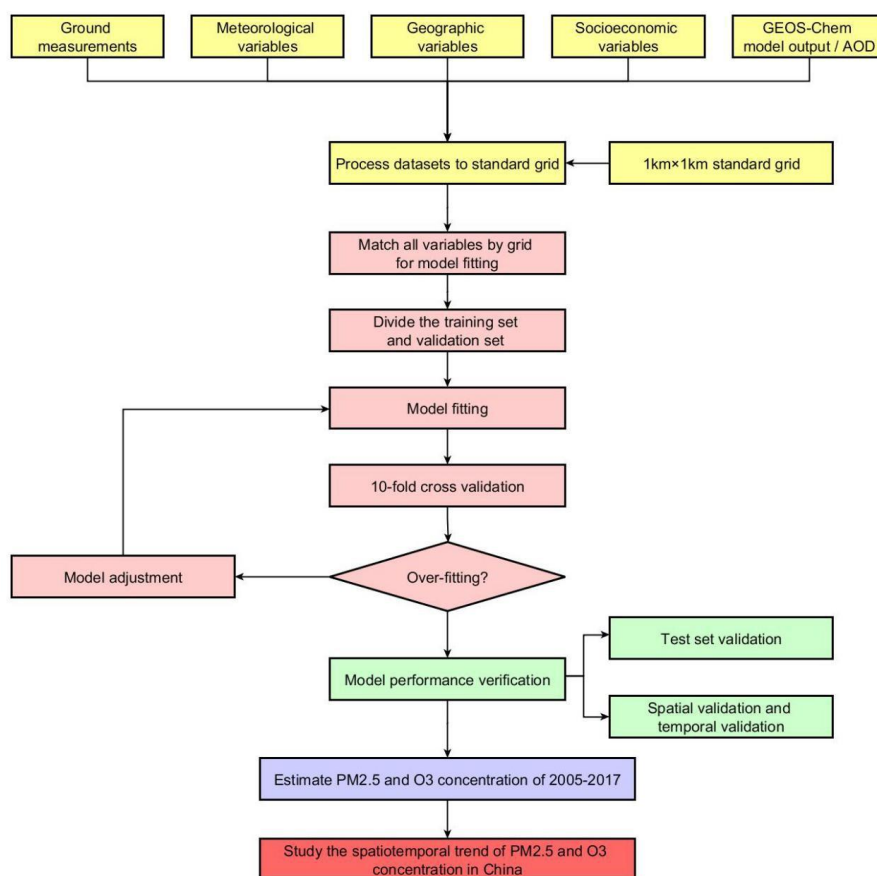
187 Based on the final models of $PM_{2.5}$ and O_3 -8hmax, we simulate the gridded daily
188 average $PM_{2.5}$ concentration and O_3 -8hmax concentration of China in 2005-2017. The
189 spatial pattern and temporal trend of $PM_{2.5}$ and O_3 -8hmax concentrations are analyzed,
190 and compared with other modeling products.

191

192 The modeling and simulations are performed in Python 2.7.13 using the



193 scikit-learn-0.20.3 and GridSearchCV packages. The workflow of this study is
194 displayed in Fig. 2.



195
196 **Fig. 2 The workflow of modeling process in the study**

197

198 3 Results and Discussion

199 A total of 981744 monitoring data records were used in the final model-fitting data set.

200 The mean \pm standard deviation of PM_{2.5} and ambient O₃ concentrations in 2013-2017

201 were $59.60 \pm 45.85 \mu\text{g}/\text{m}^3$ and $86.72 \pm 47.73 \mu\text{g}/\text{m}^3$, respectively. The results of

202 descriptive analysis for variables included in PM_{2.5} and O₃-8hamx model is shown in

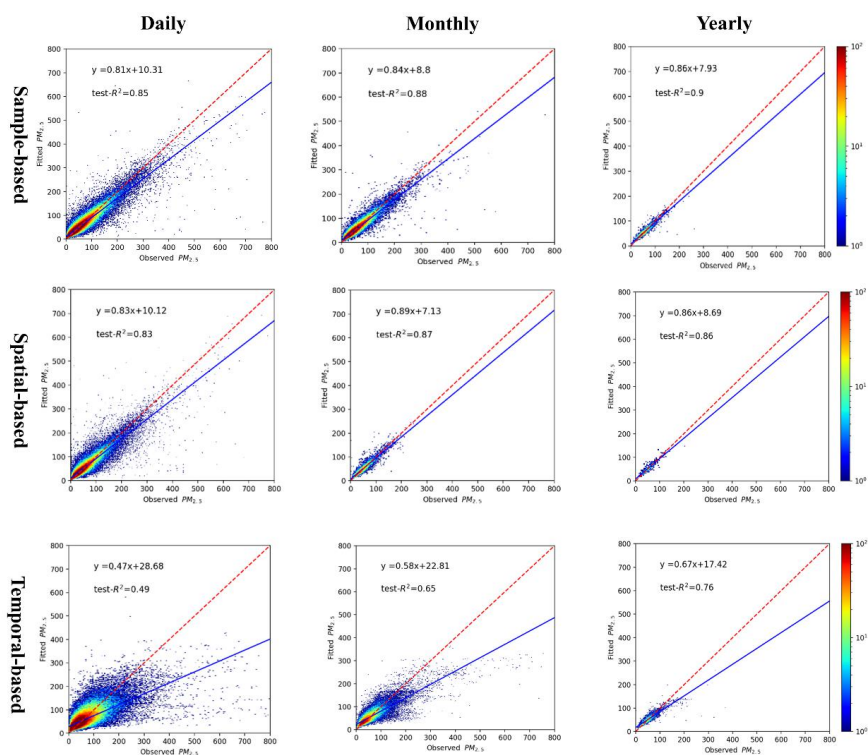


203 Table S2.

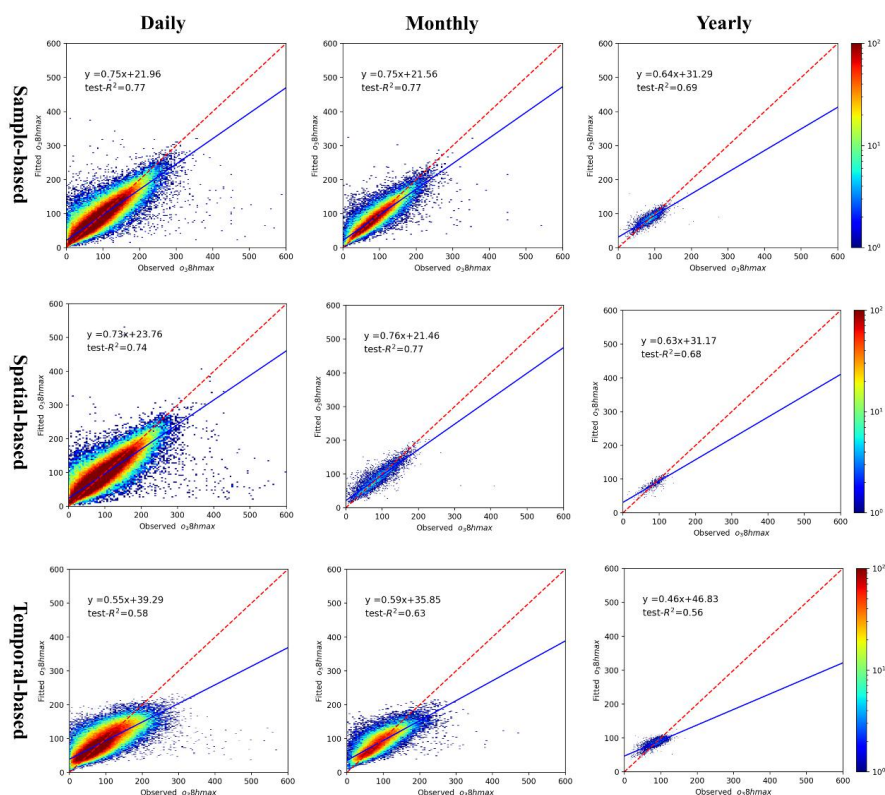
204

205 **3.1 Model fitting and validation**

206 The cross-validation results indicate that the simulated $PM_{2.5}$ and O_3 -8hmax
207 concentrations matched reasonably with the observed $PM_{2.5}$ and O_3 -8hmax
208 concentrations, with high fitted R^2 values. According to our sample-based division
209 method, the R^2 values of the simulated daily, monthly and yearly $PM_{2.5}$ concentrations
210 were 0.85, 0.88 and 0.90, respectively (Fig. 3). Likewise, the R^2 values of the
211 simulated daily, monthly and yearly O_3 -8hmax concentrations were 0.77, 0.77 and
212 0.69, respectively (Fig. 4). The RMSE and MAE for $PM_{2.5}$ in daily level were 17.72
213 and $9.37 \mu\text{g}/\text{m}^3$; for O_3 -8hmax, the values were 23.10 and $15.43 \mu\text{g}/\text{m}^3$. The model
214 performance is comparable to previous studies (Di et al., 2017; Li and Cheng, 2021;
215 Liu et al., 2020; Wei et al., 2021, 2020, 2019). At provincial/city level, $PM_{2.5}$
216 simulations of Shanghai, Beijing, Hubei, Hebei and Sichuan ranked the top 5 with
217 relatively high R^2 (≥ 0.90), while those of Tibet, Qinghai, Gansu, Anhui and Yunnan
218 were less accurate with relatively low R^2 values (< 0.70). O_3 -8hmax simulations of
219 Beijing, Chongqing, Shanghai, Tianjin and Henan ranked the top 5 with relatively
220 high R^2 values (≥ 0.83), while those of Gansu, Anhui, Heilongjiang, Guizhou and
221 Tibet were poorer with relatively low R^2 values (< 0.62) (Table S3).



222
223 **Fig. 3** The density plot of PM_{2.5} model
224 From left to right is different temporal scale: daily, monthly and yearly; From top to bottom is
225 different validation method: sample-based, spatial-based and temporal-based



226
227 **Fig. 4** The density plot of O₃-8hmax model
228 From left to right is different temporal scale: daily, monthly and yearly; From top to bottom is
229 different validation method: sample-based, spatial-based and temporal-based
230
231 The spatial and temporal R² of models explained the uncertainty of the models to
232 some content (Fig. 3 and Fig. 4). The spatial R² values for daily, monthly and yearly
233 PM_{2.5} simulation were 0.83, 0.87 and 0.86, respectively; while those of daily, monthly
234 and yearly O₃-8hmax simulations were 0.74, 0.77 and 0.68, respectively. The
235 relatively high performance demonstrates the reasonable performance of our models
236 in areas without monitoring stations. The temporal R² values of daily, monthly and
237 yearly PM_{2.5} simulations were 0.49, 0.65 and 0.76, respectively; while those of daily,



238 monthly and yearly O₃-8hmax simulations were 0.58, 0.63 and 0.56, respectively.

239 These results indicate the uncertainty of our models when modeling data in historical
240 period.

241

242 **3.2 Feature importance**

243 The feature importance of the variables in our random forest models is presented in
244 Table S4-1 and S4-2. Similar to previous studies (Chen et al., 2018; Zhan et al., 2018),
245 the meteorological factors and their lagged values can significantly affect both PM_{2.5}
246 and O₃-8hmax modeling. Moreover, the specific features for PM_{2.5} and O₃, AOD and
247 GEOS-Chem output, also demonstrated high importance in modeling work.

248

249 For PM_{2.5} modeling work (Table S4-1), the meteorological variables (boundary layer
250 height, evaporation, 2 meter dewpoint temperature) and its lagged effect were among
251 the top ten important factors, totaling 33.6% in modeling work. The lagged effects
252 greatly contributed to PM_{2.5} modeling. For example, the lag1 boundary layer height
253 ranked first (17.2%) in our study, which is similar to previous studies (Zhao et al.,
254 2019). The interpolated AOD (5.6%), DEM (4.9%) and season (3.7%) also
255 demonstrated high importance, which showed crucial effects of satellite data, terrain
256 distribution characteristics in the study area, and study period on PM_{2.5} modeling. The
257 relative contribution of land-use, NDVI, population density, road length and GDP are
258 negligible (the importance scores less than 1%). Unlike DEM, these factors are
259 subjected to the influence of socioeconomic status in study area. In the future study,



260 the integration of these factors with a higher temporal resolution might change its
261 contribution to the simulation.

262

263 The feature importance of ambient O₃ is consistent with its formation and dissipation
264 mechanism: surface solar radiation downwards and its lagged effect according for
265 38.07% in modeling work (Table S4-2). Other meteorological factors (2 meter
266 temperature, boundary layer height, 10 meter V wind component, and low cloud cover)
267 according for totaling 9.54% importance scores. Our analysis also suggests the high
268 importance of GEOS-Chem model (7.24%), altitude (1.88%), and dummy factors
269 including year (2.17%) and province (1.56%) in O₃ modeling. By contrast, the relative
270 contribution of land-use, NDVI and road length are negligible (the importance scores
271 less than 1%). The high importance rank of population and GDP might be attributed
272 to the relatively high sensitivity of O₃ to anthropogenic emission sources (compared
273 to PM_{2.5}).

274

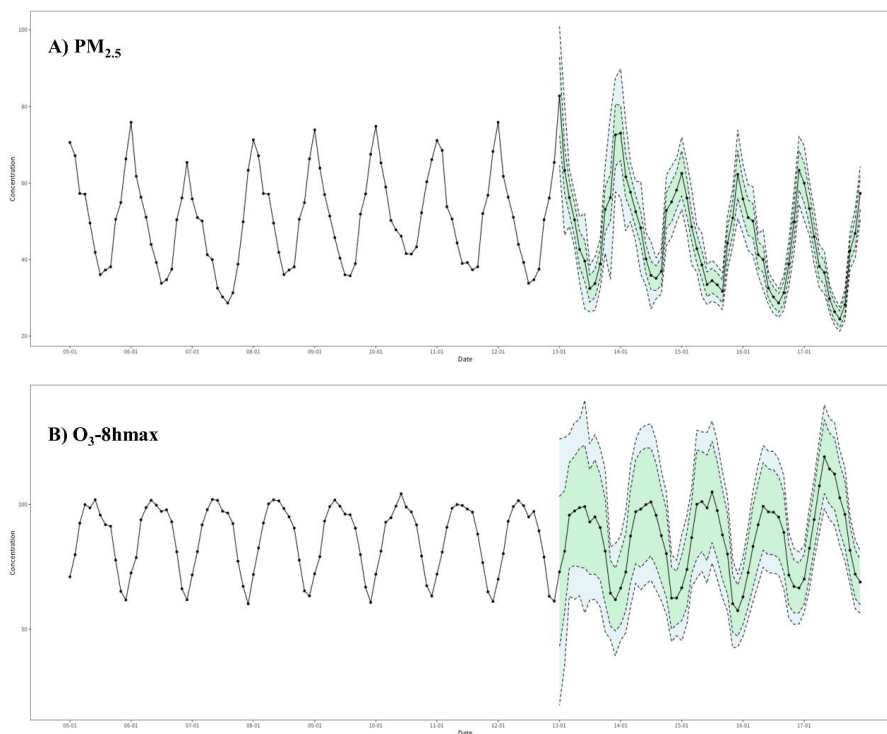
275 **3.3 The spatial characteristics and temporal trend of PM_{2.5} and ambient O₃ of**

276 **China from 2005 to 2017**

277 During 2005-2017, PM_{2.5} showed an overall downward trend, while ambient O₃
278 showed an upward trend in recent years (Fig. 5, Fig. S1 and Fig. S2). Relative to 2005,
279 PM_{2.5} concentration has increased by 2.60 µg/m³ in 2013. Nevertheless, after the
280 implementation of the *Air Pollution Prevention and Control Action Plan*, a strict
281 pollution control measure, PM_{2.5} concentration has declined by 11.041 µg/m³ in 2017



282 (relative to 2013). This has resulted in a downward trend of $PM_{2.5}$ concentration in
283 2005-2017: $PM_{2.5}$ concentration in 2017 has decreased by $8.44 \mu\text{g}/\text{m}^3$ relative to 2005
284 (Fig. 5 and Fig. S1). For O_3 -8hmax, upward barely changed. Relative to 2005,
285 O_3 -8hmax concentrations in 2013 and 2017 have increased by $0.39 \mu\text{g}/\text{m}^3$ and 7.83
286 $\mu\text{g}/\text{m}^3$, respectively. The upward trend during 2005-2017 was mostly due to the
287 significant changes between 2013 and 2017: relative to 2013, the O_3 -8hmax
288 concentration has increased by $7.44 \mu\text{g}/\text{m}^3$ in 2017 (Fig. 5 and Fig. S2). During the
289 strict pollution control period, VOC emissions were not effectively controlled could
290 be one of the main reasons. Therefore, integrated management of VOCs and NOx in
291 key industries and areas is important.



292



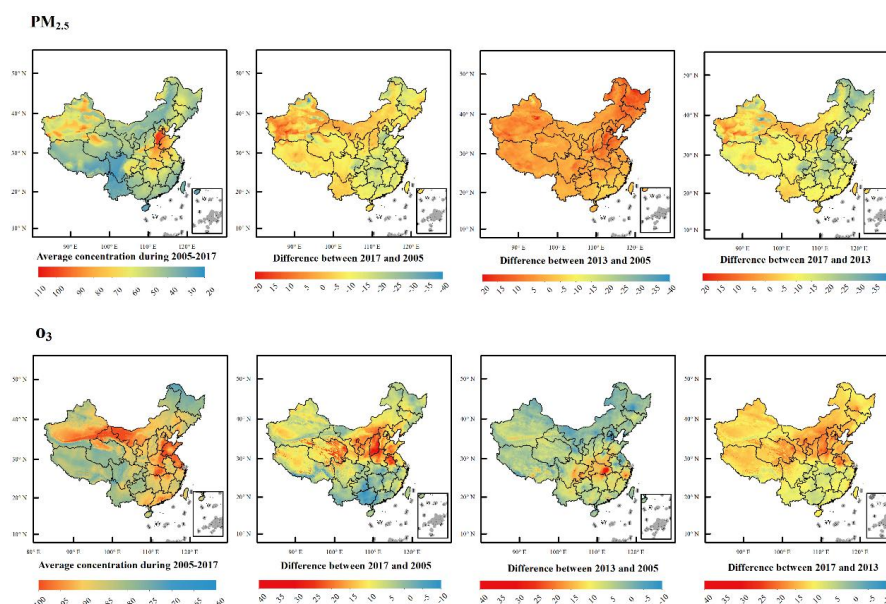
293 **Fig.5 The temporal trend of PM_{2.5} and O₃-8hmax concentration in China from 2005-2017**
294 The black dots represent the monthly average PM_{2.5} and O₃-8hmax concentration from 2005 to
295 2017, the blue color band represents the range of the monthly average PM_{2.5} and O₃-8hmax
296 concentration plus or minus the RMSE value from 2013-2017 (period with monitoring data), and
297 the green color band represents the range of the monthly average PM_{2.5} and O₃-8hmax
298 concentration plus or minus the MAE value from 2013-2017 years.
299

300 The seasonal distributions of PM_{2.5} and O₃-8hmax concentrations were obvious
301 during 2005-2017 (Fig. S3 and Fig. S4). The lowest seasonal PM_{2.5} concentration
302 occurred in summer, with an average concentration of $33.6 \pm 11.39 \mu\text{g}/\text{m}^3$; and the
303 highest seasonal PM_{2.5} concentration occurred in winter, with an average
304 concentration of $57.4 \pm 21.76 \mu\text{g}/\text{m}^3$. In winter, temperature inversion occurs frequently,
305 and the thickness of the mixed layer is low, which is not conducive to the diffusion of
306 pollutants, which leads to the accumulation of PM_{2.5} near the ground (Sun et al, 2014).
307 In opposite, the lowest seasonal O₃-8hmax concentration was in winter, with an
308 average concentration of $72.65 \pm 6.28 \mu\text{g}/\text{m}^3$; The highest seasonal O₃-8hmax
309 concentration was in summer, with an average concentration of $97.44 \pm 13.58 \mu\text{g}/\text{m}^3$.
310 Temperatures and solar radiation conditions in summer increase the incidence of
311 severe O₃ pollution events, which is consistent with its formation and dissipation
312 mechanism.
313

314 The PM_{2.5} concentrations in Beijing-Tianjin-Hebei, Chengdu-Chongqing and Xinjiang
315 regions are higher than other regions, followed by the central China. The PM_{2.5}
316 concentrations in the southwestern regions (Yunnan and Tibet) and western part of
317 Sichuan Province, are the lowest, followed by the inner-north regions and the south
318 and southeastern regions (Fig. 6 and Fig. S1; Table S5). The O₃-8hmax concentrations



319 in the Bohai Rim, Yangtze River Delta, Pearl River Delta and other economically
320 developed regions, southern Xinjiang, Inner Mongolia, and northeastern Gansu are
321 relatively high (Fig. 6 and Fig. S2; Table S5). This spatial pattern barely changed
322 during 2005-2017 (Fig. S1 and Fig. S2), but the temporal trend showed spatial
323 characteristic (Fig. 6). For $PM_{2.5}$ concentration, the above-mentioned key pollution
324 areas were severely polluted during 2005-2013. The air pollution control measures of
325 these regions were strict during 2013-2017, thus the decline was obvious. For
326 O_3 -8hmax concentration, the growth rate was not obvious (except for the eastern part
327 of Hubei Province) during 2005-2013. However, after 2013, there was a clear upward
328 trend across the country, especially in the northern China.



329
330 **Fig. 6 Simulated annual mean and difference of $PM_{2.5}$ and O_3 -8hmax concentration in China**
331 **during 2005 to 2017**

332 The first row is maps of $PM_{2.5}$ related indicators, and the second row is maps of O_3 -8hmax related
333 indicators. From left to right are average concentration during 2005-2017, the difference between



334 2017 and 2005, the difference between 2013 and 2005, and the difference between 2017 and 2013.

335

336 **3.4 Evaluation of the PM_{2.5} and O₃ concentration products with comparison with**
337 **other products**

338 Our simulation datasets include the PM_{2.5} and O₃-8hmax concentration data of China
339 in 2005-2017 with a spatial resolution of 1km×1km resolution. With high spatial and
340 temporal resolutions, our validation results are comparable with other modeling work
341 (see Table S6). Considering the future application in epidemiological research, our
342 simulation datasets would be useful: for acute effects studies, the high spatial
343 resolution would effectively reduce exposure errors; for chronic effects studies,
344 long-term exposure data is essential for the development of cohort studies.

345

346 Nevertheless, our simulation datasets also contain some limitations. First, we did not
347 use emission data in our model limited by coarse resolution. The high-resolution
348 emission inventory of China is made accessible to the public (<http://meicmodel.org/>)
349 and it can be utilized in future simulation studies to improve accuracy. Second, our
350 modeling still has spatial and temporal uncertainties. In areas where monitoring sites
351 are sparsely distributed, such as western China, it may be difficult to accurately
352 capture the association between air pollution concentrations and variables. The model
353 validation of historical period is also limited. Third, the interpolation process of model
354 features inevitably introduces some errors. Therefore, more high-quality and
355 high-resolution basic data would be needed in the future.

356



357 **4 Data availability**

358 The simulated PM_{2.5} and O₃ data are freely accessible at
359 <https://doi.org/10.5281/zenodo.4009308> (Ma et al., 2021), and the shared data set of
360 Chinese Environmental Public Health Tracking: CEPHT
361 (<https://cepht.niehs.cn:8282/developSDS3.html>).

362

363 **5 Conclusions**

364 We constructed random forest models for simulating of daily average PM_{2.5} and
365 O₃-8hmax concentrations of China during 2005-2017, with referential feature list and
366 comparable model performance. The simulation dataset would be useful for
367 supporting both long-term and short-term epidemiological studies. The model can be
368 further used for simulating daily concentrations of longer time period. The key
369 findings are summarized as follows. First, RF model proved its superiority in our
370 study and can be further used in the future simulation of air pollutant concentration.
371 Second, meteorological data is the most sensitive to PM_{2.5} and O₃ modeling. For
372 PM_{2.5} modeling work, boundary layer height, evaporation, 2 meter dewpoint
373 temperature and its lagged effects showed the highest sensitivity. For O₃ modeling
374 work, surface solar radiation downwards and its lagged effect were the most sensitive.
375 Third, PM_{2.5} concentration has trended downward in China, and the key polluted areas
376 during 2005-2013 were effectively controlled during 2013-2017. O₃ concentration has
377 trended upward in China, especially in the northern China during 2013-2017.

378



379 **Author Contribution**

380 Runmei Ma, Jie Ban and Qing Wang: Software, Investigation, Validation, Formal
381 analysis, Data curation, Writing - original draft. Yayi Zhang: Formal analysis,
382 Visualization. Yang Yang, Shenshen Li and Wenjiao Shi: Methodology, Writing -
383 Review & Editing. Tiantian Li: Conceptualization, Methodology, Writing - Review &
384 Editing.

385

386 **Competing Interests**

387 The authors declare that they have no conflict of interest.

388

389 **Acknowledgements**

390 This work was funded by grants from National Natural Science Foundation of China
391 (Grant No. 92043301 and 42071433).

392

393 **Reference**

- 394 Breiman, L., 2001. Random forest. *Machine Learning* 45, 5–32.
- 395 Chen, G., Li, S., Knibbs, L.D., Hamm, N.A.S., Cao, W., Li, T., Guo, J., Ren, H.,
396 Abramson, M.J., Guo, Y., 2018. A machine learning method to estimate
397 PM2.5 concentrations across China with remote sensing, meteorological and
398 land use information. *Science of The Total Environment* 636, 52–60.
399 <https://doi.org/10.1016/j.scitotenv.2018.04.251>
- 400 Chen, Z.-Y., Zhang, T.-H., Zhang, R., Zhu, Z.-M., Yang, J., Chen, P.-Y., Ou, C.-Q.,
401 Guo, Y., 2019. Extreme gradient boosting model to estimate PM2.5
402 concentrations with missing-filled satellite data in China. *Atmospheric*
403 *Environment* 202, 180–189. <https://doi.org/10.1016/j.atmosenv.2019.01.027>
- 404 Di, Q., Rowland, S., Koutrakis, P., Schwartz, J., 2017. A hybrid model for spatially
405 and temporally resolved ozone exposures in the continental United States.
406 *Journal of the Air & Waste Management Association* 67, 39–52.
407 <https://doi.org/10.1080/10962247.2016.1200159>



- 408 Health Effects Institute, 2020. State of Global Air 2020 28.
- 409 Li, T., Cheng, X., 2021. Estimating daily full-coverage surface ozone concentration
410 using satellite observations and a spatiotemporally embedded deep learning
411 approach. *International Journal of Applied Earth Observation and*
412 *Geoinformation* 101, 102356. <https://doi.org/10.1016/j.jag.2021.102356>
- 413 Li, T., Shen, H., Yuan, Q., Zhang, X., Zhang, L., 2017. Estimating Ground-Level PM
414 _{2.5} by Fusing Satellite and Station Observations: A Geo-Intelligent Deep
415 Learning Approach: Deep Learning for PM _{2.5} Estimation. *Geophys. Res. Lett.*
416 44, 11,985-11,993. <https://doi.org/10.1002/2017GL075710>
- 417 Liu, R., Ma, Z., Liu, Y., Shao, Y., Zhao, W., Bi, J., 2020. Spatiotemporal distributions
418 of surface ozone levels in China from 2005 to 2017: A machine learning
419 approach. *Environment International* 142, 105823.
420 <https://doi.org/10.1016/j.envint.2020.105823>
- 421 Ma, R., Ban, J., Wang, Q., Zhang, Y., Li, T., 2021. Full-coverage 1 km daily ambient
422 PM_{2.5} and O₃ concentrations of China in 2005-2017 based on multi-variable
423 random forest model.
- 424 Ma, R., Ban, J., Wang, Q., Zhang, Y., Li, T., 2021. Random Forest Model based Fine
425 Scale Spatiotemporal O₃ Trends in the Beijing-Tianjin-Hebei region in China,
426 2010 to 2017. *Environmental Pollution* 116635.
- 427 Murray, C.J.L., Aravkin, A.Y., Zheng, P., Abbafati, C., Abbas, K.M.,
428 Abbasi-Kangevari, M., Abd-Allah, F., Abdelalim, A., Abdollahi, M.,
429 Abdollahpour, I., Abegaz, K.H., Abolhassani, H., Aboyans, V., Abreu, L.G.,
430 Abrigo, M.R.M., Abualhasan, A., Abu-Raddad, L.J., Abushouk, A.I., Adabi,
431 M., Adekanmbi, V., Adeoye, A.M., Adetokunboh, O.O., Adham, D., Advani,
432 S.M., Agarwal, G., Aghamir, S.M.K., Agrawal, A., Ahmad, T., Ahmadi, K.,
433 Ahmadi, M., Ahmadieh, H., Ahmed, M.B., Akalu, T.Y., Akinyemi, R.O.,
434 Akinyemiju, T., Akombi, B., Akunna, C.J., Alahdab, F., Al-Aly, Z., Alam, K.,
435 Alam, S., Alam, T., Alanezi, F.M., Alanzi, T.M., Alemu, B. wassihun,
436 Alhabib, K.F., Ali, M., Ali, S., Alicandro, G., Alinia, C., Alipour, V., Alizade,
437 H., Aljunid, S.M., Alla, F., Allebeck, P., Almasi-Hashiani, A., Al-Mekhlafi,
438 H.M., Alonso, J., Altirkawi, K.A., Amini-Rarani, M., Amiri, F., Amugsi, D.A.,
439 Ancuceanu, R., Anderlini, D., Anderson, J.A., Andrei, C.L., Andrei, T., Angus,
440 C., Anjomshoa, M., Ansari, F., Ansari-Moghaddam, A., Antonazzo, I.C.,
441 Antonio, C.A.T., Antony, C.M., Antriyandarti, E., Anvari, D., Anwer, R.,
442 Appiah, S.C.Y., Arabloo, J., Arab-Zozani, M., Ariani, F., Armoon, B., Ämrlöv,
443 J., Arzani, A., Asadi-Aliabadi, M., Asadi-Pooya, A.A., Ashbaugh, C., Assmus,
444 M., Atafar, Z., Atnafu, D.D., Atout, M.M.W., Ausloos, F., Ausloos, M., Ayala
445 Quintanilla, B.P., Ayano, G., Ayanore, M.A., Azari, S., Azarian, G., Azene,
446 Z.N., Badawi, A., Badiye, A.D., Bahrami, M.A., Bakhshaei, M.H., Bakhtiari,
447 A., Bakkannavar, S.M., Baldasseroni, A., Ball, K., Ballew, S.H., Balzi, D.,
448 Banach, M., Banerjee, S.K., Bante, A.B., Baraki, A.G., Barker-Collo, S.L.,
449 Bärnighausen, T.W., Barrero, L.H., Barthelemy, C.M., Barua, L., Basu, S.,
450 Baune, B.T., Bayati, M., Becker, J.S., Bedi, N., Beghi, E., Béjot, Y., Bell,
451 M.L., Bennitt, F.B., Bensenor, I.M., Berhe, K., Berman, A.E., Bhagavathula,



452 A.S., Bhageerathy, R., Bhala, N., Bhandari, D., Bhattacharyya, K., Bhutta,
453 Z.A., Bijani, A., Bikbov, B., Bin Sayeed, M.S., Biondi, A., Birihane, B.M.,
454 Bisignano, C., Biswas, R.K., Bitew, H., Bohlouli, S., Bohluli, M.,
455 Boon-Dooley, A.S., Borges, G., Borzi, A.M., Borzouei, S., Bosetti, C.,
456 Boufous, S., Braithwaite, D., Breitborde, N.J.K., Breitner, S., Brenner, H.,
457 Briant, P.S., Briko, A.N., Briko, N.I., Britton, G.B., Bryazka, D., Bumgarner,
458 B.R., Burkart, K., Burnett, R.T., Burugina Nagaraja, S., Butt, Z.A., Caetano
459 dos Santos, F.L., Cahill, L.E., Cámera, L.L.A., Campos-Nonato, I.R.,
460 Cárdenas, R., Carreras, G., Carrero, J.J., Carvalho, F., Castaldelli-Maia, J.M.,
461 Castañeda-Orjuela, C.A., Castelpietra, G., Castro, F., Causey, K., Cederroth,
462 C.R., Cercy, K.M., Cerin, E., Chandan, J.S., Chang, K.-L., Charlson, F.J.,
463 Chattu, V.K., Chaturvedi, S., Cherbuin, N., Chimed-Ochir, O., Cho, D.Y.,
464 Choi, J.-Y.J., Christensen, H., Chu, D.-T., Chung, M.T., Chung, S.-C.,
465 Cicuttini, F.M., Ciobanu, L.G., Cirillo, M., Classen, T.K.D., Cohen, A.J.,
466 Compton, K., Cooper, O.R., Costa, V.M., Cousin, E., Cowden, R.G., Cross,
467 D.H., Cruz, J.A., Dahlawi, S.M.A., Damasceno, A.A.M., Damiani, G.,
468 Dandona, L., Dandona, R., Dangel, W.J., Danielsson, A.-K., Dargan, P.I.,
469 Darwesh, A.M., Daryani, A., Das, J.K., Das Gupta, R., das Neves, J.,
470 Dávila-Cervantes, C.A., Davitoiu, D.V., De Leo, D., Degenhardt, L., DeLang,
471 M., Dellavalle, R.P., Demeke, F.M., Demoz, G.T., Demsie, D.G.,
472 Denova-Gutiérrez, E., Dervenis, N., Dhungana, G.P., Dianatinasab, M., Dias
473 da Silva, D., Diaz, D., Dibaji Forooshani, Z.S., Djalalinia, S., Do, H.T.,
474 Dokova, K., Dorostkar, F., Doshmangir, L., Driscoll, T.R., Duncan, B.B.,
475 Duraes, A.R., Eagan, A.W., Edvardsson, D., El Nahas, N., El Sayed, I., El
476 Tantawi, M., Elbarazi, I., Elgendy, I.Y., El-Jaafary, S.I., Elyazar, I.R.,
477 Emmons-Bell, S., Erskine, H.E., Eskandarieh, S., Esmailnejad, S.,
478 Esteghamati, A., Estep, K., Etemadi, A., Etisso, A.E., Fanzo, J., Farahmand,
479 M., Fareed, M., Faridnia, R., Farioli, A., Faro, A., Faruque, M., Farzadfar, F.,
480 Fattahi, N., Fazlzadeh, M., Feigin, V.L., Feldman, R., Fereshtehnejad, S.-M.,
481 Fernandes, E., Ferrara, G., Ferrari, A.J., Ferreira, M.L., Filip, I., Fischer, F.,
482 Fisher, J.L., Flor, L.S., Foigt, N.A., Folleyan, M.O., Fomenkov, A.A., Force,
483 L.M., Foroutan, M., Franklin, R.C., Freitas, M., Fu, W., Fukumoto, T.,
484 Furtado, J.M., Gad, M.M., Gakidou, E., Gallus, S., Garcia-Basteiro, A.L.,
485 Gardner, W.M., Geberemariam, B.S., Gebreslassie, A.A.A.A., Geremew, A.,
486 Gershberg Hayoon, A., Gething, P.W., Ghadimi, M., Ghadiri, K., Ghaffarifar,
487 F., Ghafourifard, M., Ghamari, F., Ghashghaee, A., Ghiasvand, H., Ghith, N.,
488 Gholamian, A., Ghosh, R., Gill, P.S., Ginindza, T.G.G., Giussani, G.,
489 Gnedovskaya, E.V., Goharinezhad, S., Gopalani, S.V., Gorini, G., Goudarzi,
490 H., Goulart, A.C., Greaves, F., Grivna, M., Grosso, G., Gubari, M.I.M.,
491 Gughani, H.C., Guimaraes, R.A., Guled, R.A., Guo, G., Guo, Y., Gupta, R.,
492 Gupta, T., Haddock, B., Hafezi-Nejad, N., Hafiz, A., Haj-Mirzaian, Arvin,
493 Haj-Mirzaian, Arya, Hall, B.J., Halvaei, I., Hamadeh, R.R., Hamidi, S.,
494 Hammer, M.S., Hankey, G.J., Haririan, H., Haro, J.M., Hasaballah, A.I.,
495 Hasan, M.M., Hasanpoor, E., Hashi, A., Hassanipour, S., Hassankhani, H.,



496 Havmoeller, R.J., Hay, S.I., Hayat, K., Heidari, G., Heidari-Soureshjani, R.,
497 Henrikson, H.J., Herbert, M.E., Herteliu, C., Heydarpour, F., Hird, T.R., Hoek,
498 H.W., Holla, R., Hoogar, P., Hosgood, H.D., Hossain, N., Hosseini, M.,
499 Hosseinzadeh, M., Hostiuc, M., Hostiuc, S., Househ, M., Hsairi, M., Hsieh,
500 V.C., Hu, G., Hu, K., Huda, T.M., Humayun, A., Huynh, C.K., Hwang, B.-F.,
501 Iannucci, V.C., Ibitoye, S.E., Ikeda, N., Ikuta, K.S., Ilesanmi, O.S., Ilic, I.M.,
502 Ilic, M.D., Inbaraj, L.R., Ippolito, H., Iqbal, U., Irvani, S.S.N., Irvine, C.M.S.,
503 Islam, M.M., Islam, S.M.S., Iso, H., Ivers, R.Q., Iwu, C.C.D., Iwu, C.J., Iyamu,
504 I.O., Jaafari, J., Jacobsen, K.H., Jafari, H., Jafarina, M., Jahani, M.A.,
505 Jakovljevic, M., Jalilian, F., James, S.L., Janjani, H., Javaheri, T., Javidnia, J.,
506 Jeemon, P., Jenabi, E., Jha, R.P., Jha, V., Ji, J.S., Johansson, L., John, O.,
507 John-Akinola, Y.O., Johnson, C.O., Jonas, J.B., Joukar, F., Jozwiak, J.J.,
508 Jürisson, M., Kabir, A., Kabir, Z., Kalani, H., Kalani, R., Kalankesh, L.R.,
509 Kalhor, R., Kanchan, T., Kapoor, N., Karami Matin, B., Karch, A., Karim,
510 M.A., Kassa, G.M., Katikireddi, S.V., Kayode, G.A., Kazemi Karyani, A.,
511 Keiyoro, P.N., Keller, C., Kemmer, L., Kendrick, P.J., Khalid, N.,
512 Khammarnia, M., Khan, E.A., Khan, M., Khatib, K., Khater, M.M., Khatib,
513 M.N., Khayamzadeh, M., Khazaei, S., Kielling, C., Kim, Y.J., Kimokoti, R.W.,
514 Kisa, A., Kisa, S., Kivimäki, M., Knibbs, L.D., Knudsen, A.K.S., Kocarnik,
515 J.M., Kochhar, S., Kopec, J.A., Korshunov, V.A., Koul, P.A., Koyanagi, A.,
516 Kraemer, M.U.G., Krishan, K., Krohn, K.J., Kromhout, H., Kuate Defo, B.,
517 Kumar, G.A., Kumar, V., Kurmi, O.P., Kusuma, D., La Vecchia, C., Lacey, B.,
518 Lal, D.K., Lalloo, R., Lallukka, T., Lami, F.H., Landires, I., Lang, J.J., Langan,
519 S.M., Larsson, A.O., Lasrado, S., Lauriola, P., Lazarus, J.V., Lee, P.H., Lee,
520 S.W.H., LeGrand, K.E., Leigh, J., Leonardi, M., Lescinsky, H., Leung, J.,
521 Levi, M., Li, S., Lim, L.-L., Linn, S., Liu, Shiwei, Liu, Simin, Liu, Y., Lo, J.,
522 Lopez, A.D., Lopez, J.C.F., Lopukhov, P.D., Lorkowski, S., Lotufo, P.A., Lu,
523 A., Lugo, A., Maddison, E.R., Mahasha, P.W., Mahdavi, M.M., Mahmoudi,
524 M., Majeed, A., Maleki, A., Maleki, S., Malekzadeh, R., Malta, D.C., Mamun,
525 A.A., Manda, A.L., Manguerra, H., Mansour-Ghanaei, F., Mansouri, B.,
526 Mansournia, M.A., Mantilla Herrera, A.M., Maravilla, J.C., Marks, A., Martin,
527 R.V., Martini, S., Martins-Melo, F.R., Masaka, A., Masoumi, S.Z., Mathur,
528 M.R., Matsushita, K., Maulik, P.K., McAlinden, C., McGrath, J.J., McKee, M.,
529 Mehdiratta, M.M., Mehri, F., Mehta, K.M., Memish, Z.A., Mendoza, W.,
530 Menezes, R.G., Mengesha, E.W., Mereke, A., Mereta, S.T., Meretoja, A.,
531 Meretoja, T.J., Mestrovic, T., Miazgowski, B., Miazgowski, T., Michalek,
532 I.M., Miller, T.R., Mills, E.J., Mini, G., Miri, M., Mirica, A., Mirrakhimov,
533 E.M., Mirzaei, H., Mirzaei, M., Mirzaei, R., Mirzaei-Alavijeh, M., Misganaw,
534 A.T., Mithra, P., Moazen, B., Mohammad, D.K., Mohammad, Y., Mohammad
535 Gholi Mezerji, N., Mohammadian-Hafshejani, A., Mohammadifard, N.,
536 Mohammadpourhodki, R., Mohammed, A.S., Mohammed, H., Mohammed,
537 J.A., Mohammed, S., Mokdad, A.H., Molokhia, M., Monasta, L., Mooney,
538 M.D., Moradi, G., Moradi, M., Moradi-Lakeh, M., Moradzadeh, R., Moraga,
539 P., Morawska, L., Morgado-da-Costa, J., Morrison, S.D., Mosapour, A.,



540 Mosser, J.F., Mouodi, S., Mousavi, S.M., Mousavi Khaneghah, A., Mueller,
541 U.O., Mukhopadhyay, S., Mullany, E.C., Musa, K.I., Muthupandian, S.,
542 Nabhan, A.F., Naderi, M., Nagarajan, A.J., Nagel, G., Naghavi, M.,
543 Naghshtabrizi, B., Naimzada, M.D., Najafi, F., Nangia, V., Nansseu, J.R.,
544 Naserbakht, M., Nayak, V.C., Negoi, I., Ngunjiri, J.W., Nguyen, C.T., Nguyen,
545 H.L.T., Nguyen, M., Nigatu, Y.T., Nikbakhsh, R., Nixon, M.R., Nnaji, C.A.,
546 Nomura, S., Norrving, B., Noubiap, J.J., Nowak, C., Nunez-Samudio, V.,
547 Oțoiu, A., Oancea, B., Odell, C.M., Ogbo, F.A., Oh, I.-H., Okunga, E.W.,
548 Oladnabi, M., Olagunju, A.T., Olusanya, B.O., Olusanya, J.O., Omer, M.O.,
549 Ong, K.L., Onwujekwe, O.E., Orpana, H.M., Ortiz, A., Osarenotor, O., Osei,
550 F.B., Ostroff, S.M., Otstavnov, N., Otstavnov, S.S., Øverland, S., Owolabi,
551 M.O., P A, M., Padubidri, J.R., Palladino, R., Panda-Jonas, S., Pandey, A.,
552 Parry, C.D.H., Pasovic, M., Pasupula, D.K., Patel, S.K., Pathak, M., Patten,
553 S.B., Patton, G.C., Pazoki Toroudi, H., Peden, A.E., Pennini, A., Pepito,
554 V.C.F., Peprah, E.K., Pereira, D.M., Pesudovs, K., Pham, H.Q., Phillips, M.R.,
555 Piccinelli, C., Pilz, T.M., Piradov, M.A., Pirsaeheb, M., Plass, D., Polinder, S.,
556 Polkinghorne, K.R., Pond, C.D., Postma, M.J., Pourjafar, H., Pourmalek, F.,
557 Poznańska, A., Prada, S.I., Prakash, V., Pribadi, D.R.A., Pupillo, E., Quazi
558 Syed, Z., Rabiee, M., Rabiee, N., Radfar, A., Rafiee, A., Raggi, A., Rahman,
559 M.A., Rajabpour-Sanati, A., Rajati, F., Rakovac, I., Ram, P., Ramezanzadeh,
560 K., Ranabhat, C.L., Rao, P.C., Rao, S.J., Rashedi, V., Rathi, P., Rawaf, D.L.,
561 Rawaf, S., Rawal, L., Rawassizadeh, R., Rawat, R., Razo, C., Redford, S.B.,
562 Reiner, R.C., Reitsma, M.B., Remuzzi, G., Renjith, V., Renzaho, A.M.N.,
563 Resnikoff, S., Rezaei, Negar, Rezaei, Nima, Rezapour, A., Rhinehart, P.-A.,
564 Riahi, S.M., Ribeiro, D.C., Ribeiro, D., Rickard, J., Rivera, J.A., Roberts,
565 N.L.S., Rodríguez-Ramírez, S., Roeber, L., Ronfani, L., Room, R., Roshandel,
566 G., Roth, G.A., Rothenbacher, D., Rubagotti, E., Rwegera, G.M., Sabour, S.,
567 Sachdev, P.S., Saddik, B., Sadeghi, E., Sadeghi, M., Saeedi, R., Saeedi
568 Moghaddam, S., Safari, Y., Safi, S., Safiri, S., Sagar, R., Sahebkar, A., Sajadi,
569 S.M., Salam, N., Salamati, P., Salem, H., Salem, M.R.R., Salimzadeh, H.,
570 Salman, O.M., Salomon, J.A., Samad, Z., Samadi Kafil, H., Sambala, E.Z.,
571 Samy, A.M., Sanabria, J., Sánchez-Pimienta, T.G., Santomauro, D.F., Santos,
572 I.S., Santos, J.V., Santric-Milicevic, M.M., Saraswathy, S.Y.I.,
573 Sarmiento-Suárez, R., Sarrafzadegan, N., Sartorius, B., Sarveazad, A., Sathian,
574 B., Sathish, T., Sattin, D., Saxena, S., Schaeffer, L.E., Schiavolin, S., Schlaich,
575 M.P., Schmidt, M.I., Schutte, A.E., Schwebel, D.C., Schwendicke, F., Senbeta,
576 A.M., Senthilkumaran, S., Sepanlou, S.G., Serdar, B., Serre, M.L., Shadid, J.,
577 Shafaat, O., Shahabi, S., Shaheen, A.A., Shaikh, M.A., Shalash, A.S.,
578 Shams-Beyranvand, M., Shamsizadeh, M., Sharafi, K., Sheikh, A.,
579 Sheikhtaheri, A., Shibuya, K., Shield, K.D., Shigematsu, M., Shin, J.I., Shin,
580 M.-J., Shiri, R., Shirkoohi, R., Shuval, K., Siabani, S., Sierpinski, R.,
581 Sigfusdottir, I.D., Sigurvinsdottir, R., Silva, J.P., Simpson, K.E., Singh, J.A.,
582 Singh, P., Skiadarsi, E., Skou, S.T.S., Skryabin, V.Y., Smith, E.U.R., Soheili,
583 A., Soltani, S., Soofi, M., Sorensen, R.J.D., Soriano, J.B., Sorrie, M.B.,



- 584 Soshnikov, S., Soyiri, I.N., Spencer, C.N., Spotin, A., Sreeramareddy, C.T.,
585 Srinivasan, V., Stanaway, J.D., Stein, C., Stein, D.J., Steiner, C., Stockfelt, L.,
586 Stokes, M.A., Straif, K., Stubbs, J.L., Sufiyan, M.B., Suleria, H.A.R.,
587 Suliankatchi Abdulkader, R., Sulo, G., Sultan, I., Szumowski, Ł.,
588 Tabarés-Seisdedos, R., Tabb, K.M., Tabuchi, T., Taherkhani, A., Tajdini, M.,
589 Takahashi, K., Takala, J.S., Tamiru, A.T., Taveira, N., Tehrani-Banihashemi,
590 A., Temsah, M.-H., Tesema, G.A., Tessema, Z.T., Thurston, G.D., Titova,
591 M.V., Tohidinik, H.R., Tonelli, M., Topor-Madry, R., Topouzis, F., Torre,
592 A.E., Touvier, M., Tovani-Palone, M.R.R., Tran, B.X., Travillian, R.,
593 Tsatsakis, A., Tudor Car, L., Tyrovolas, S., Uddin, R., Umeokonkwo, C.D.,
594 Unnikrishnan, B., Upadhyay, E., Vacante, M., Valdez, P.R., van Donkelaar,
595 A., Vasankari, T.J., Vasseghian, Y., Veisani, Y., Venketasubramanian, N.,
596 Violante, F.S., Vlassov, V., Vollset, S.E., Vos, T., Vukovic, R., Waheed, Y.,
597 Wallin, M.T., Wang, Y., Wang, Y.-P., Watson, A., Wei, J., Wei, M.Y.W.,
598 Weintraub, R.G., Weiss, J., Werdecker, A., West, J.J., Westerman, R.,
599 Whisnant, J.L., Whiteford, H.A., Wiens, K.E., Wolfe, C.D.A., Wozniak, S.S.,
600 Wu, A.-M., Wu, J., Wulf Hanson, S., Xu, G., Xu, R., Yadgir, S., Yahyazadeh
601 Jabbari, S.H., Yamagishi, K., Yaminfirooz, M., Yano, Y., Yaya, S.,
602 Yazdi-Fezabadi, V., Yeheyis, T.Y., Yilgwan, C.S., Yilma, M.T., Yip, P.,
603 Yonemoto, N., Younis, M.Z., Younker, T.P., Yousefi, B., Yousefi, Z.,
604 Yousefinezhadi, T., Yousuf, A.Y., Yu, C., Yusefzadeh, H., Zahirian
605 Moghadam, T., Zamani, M., Zamanian, M., Zandian, H., Zastrozhin, M.S.,
606 Zhang, Y., Zhang, Z.-J., Zhao, J.T., Zhao, X.-J.G., Zhao, Y., Zhou, M.,
607 Ziapour, A., Zimsen, S.R.M., Brauer, M., Afshin, A., Lim, S.S., 2020. Global
608 burden of 87 risk factors in 204 countries and territories, 1990–2019: a
609 systematic analysis for the Global Burden of Disease Study 2019. *The Lancet*
610 396, 1223–1249. [https://doi.org/10.1016/S0140-6736\(20\)30752-2](https://doi.org/10.1016/S0140-6736(20)30752-2)
611 Wei, J., Huang, W., Li, Z., Xue, W., Peng, Y., Sun, L., Cribb, M., 2019. Estimating
612 1-km-resolution PM_{2.5} concentrations across China using the space-time
613 random forest approach. *Remote Sensing of Environment* 231, 111221.
614 <https://doi.org/10.1016/j.rse.2019.111221>
615 Wei, J., Li, Z., Cribb, M., Huang, W., Xue, W., Sun, L., Guo, J., Peng, Y., Li, J.,
616 Lyapustin, A., Liu, L., Wu, H., Song, Y., 2020. Improved 1 km resolution
617 PM_{2.5} estimates across China using enhanced
618 space–time extremely randomized trees. *Atmos. Chem. Phys.* 20, 3273–3289.
619 <https://doi.org/10.5194/acp-20-3273-2020>
620 Wei, J., Li, Z., Lyapustin, A., Sun, L., Peng, Y., Xue, W., Su, T., Cribb, M., 2021.
621 Reconstructing 1-km-resolution high-quality PM_{2.5} data records from 2000 to
622 2018 in China: spatiotemporal variations and policy implications. *Remote*
623 *Sensing of Environment* 252, 112136.
624 <https://doi.org/10.1016/j.rse.2020.112136>
625 Zhan, Y., Luo, Y., Deng, X., Grieneisen, M.L., Zhang, M., Di, B., 2018.
626 Spatiotemporal prediction of daily ambient ozone levels across China using
627 random forest for human exposure assessment. *Environmental Pollution* 233,



628 464–473. <https://doi.org/10.1016/j.envpol.2017.10.029>
629 Zhao, C., Wang, Q., Ban, J., Liu, Z., Li, T., 2019. Estimating the daily PM2.5
630 concentration in the Beijing-Tianjin-Hebei region using a random forest model
631 with a $0.01^\circ \times 0.01^\circ$ spatial resolution. *Environment international* 134,
632 105297.
633